Assessment of the Fracture Behavior of an Asymmetrically Loaded Cantilever Composite Structure

Baoxiang Shan

Assimina A. Pelegri
e-mail: pelegri@jove.rutgers.edu

Rutgers, The State University of New Jersey,
Department of Mechanical and Aerospace Engineering,
98 Brett Road,
Piscataway, NJ 08854-8058 USA

The complex fracture behavior of a cross-ply composite cantilever beam with artificially embedded delamination is investigated analytically, numerically, and experimentally. The analysis of the cantilever beam is divided into two geometric configurations: the global bending of the undelaminated cantilever, and the local buckling of the delaminated part. A finite element model developed in ANSYS is used to concurrently analyze the effects of contact zone and delamination in the aforementioned asymmetrically loaded structure. The obtained experimental data are correlated and compared with the findings of the FEM simulations. All numerical, analytical, and experimental results illustrate that the fracture behavior of the laminate cantilever beam is dominated by mode II, mainly due to the effect of a large contact zone. The latter is determined by geometric and loading parameters. The dominance of mode II over mode I, leads to the initiation and propagation of an interfacial crack rather than an intralayer one. Furthermore, experimental evidence indicates that crack kinking during propagation depends on the architecture of the specimens. [DOI: 10.1115/1.1605108]

Introduction

It is well established that delaminations are in the forefront of composite structures' catastrophic modes of damage. As such, delaminations limit the application of composites in fields where their properties of high stiffness-to-weight and high strength-to-weight ratios are highly desirable.

Analysis of the structural degradation and failure of composite structures due to delamination are referenced with the appearance of man-made composite. Sanford [1,2] illustrated that Linear Elastic Fracture Mechanics (LEFM) is mainly founded on the analysis of stresses around tips of cracks and defects. LEFM offers a good way to analyze and characterize the fracture behavior in isotropic and homogeneous solid media. It also causes unexplainable characteristics of oscillation and penetration of the crack flanks, when it is employed in two dissimilar media. The in-plane uni-axial compression of a delaminated composite structure using the von Karman kinetic approach was studied by Sheinman [3,4], while similar cases were investigated by Simitses and Yin [5,6] using Bernoulli-Euler beam theory, by Kardomateas [7] utilizing a nonlinear elliptic integration, and by Suemasu [8,9] by employing the Rayleigh-Ritz method. The above studies did not consider the effect of contact zone, or assume that it had no major effect, and investigated the standard cases of double cantilever beam (DCB), mixed mode bending (MMB), uni-axial compression, and three or four-point bending. Comninou and Dundurs [10–11] in 1979, as well as Antipov [12] and Audoly [13] more recently, introduced the contact zone by depicting it as a series of dislocations on the crack flanks. However, the model of small contact zone was just limited to simply idealistic structures.

Whitcomb [14] and Moradi [15] illustrated the effectiveness of numerical methods by investigating the effect of a small contact zone on fracture and fatigue performance of symmetric specimens and symmetric loading. To this extent, Whitcomb used finite elements while Moradi employed differential quadratures. Yeh [16,17] examined the effect of a large contact zone in the cases of delaminated cantilever beams and delaminated bending plates by nonlinear finite element method. Yeh's major work was focused on the characteristics of the contact zone and its effect on the mechanical behavior, such as bending and end-displacements. The fracture and fatigue behaviors, of most interest to the present researchers, were not examined. Furthermore, the specimens in his experiments were unidirectional (0 deg), which hided the complex issue of trajectory selection during crack propagation.

The following work is to investigate the formation of a large contact zone during local buckling deformation, and its effect on the fracture behavior of a delaminated composite cantilever beam by theoretical, numerical, and experimental means.

Finite Element Model

The structural geometry adopted in the current study, is similar to the one found in Yeh [16], see Fig. 1. For the delaminated cantilever part of Fig. 1, a two-dimensional finite element model (FEM) was developed in ANSYS 6.1. The model's geometry and material properties are listed in Table 1 and Table 2, respectively. The FEM model includes: (i) a stress-concentrated point at each end of the delamination, which produced singular elements around it (shown in Fig. 2), and (ii) a contact pair, which preceded the delamination and introduced special contact elements between adjacent nodes on the delamination's flanks. The effects of contact and friction were incorporated into the analysis by an augmented Lagrange method. The unit element employed was a 6-node triangular element PLANE 2 [18]. In practice, we also introduced a small area around each concentrated point in order to obtain a better meshing. The meshes were generated automatically by ANSYS. Upon load application, buckling and post-buckling of the delaminated part occurred, leading to large deformations and contact effects. The resulting geometric nonlinearity was accounted for in the FEM analysis.

First, the case without contact and friction on the delamination was considered. The result of the out-of-plane deformation indicated an apparent penetration between the two sides of the delamination at its inner end, as illustrated in Fig. 3. This observation corroborates the initiative for inclusion of contact and frictional

Contributed by the Materials Division for publication in the JOURNAL OF ENGINEERING MATERIALS AND TECHNOLOGY. Manuscript received by the Materials Division January 21, 2003; revision received June 17, 2003. Associate Editor: A. Karlsson.

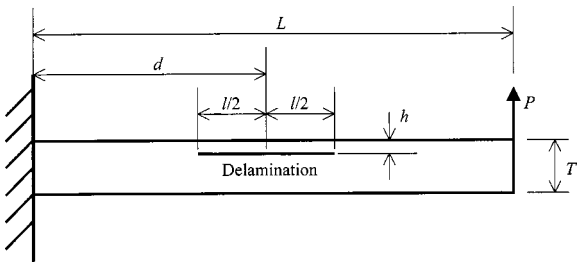

Fig. 1 Geometry of the delaminated cantilever

effects. Second, the analysis of a model incorporating contact and friction on the sides of delamination was implemented. We analyzed the following cases: (i) no delamination, (ii) delaminated model without contact zone, and (iii) delaminated model with contact zone, and compared their results, see Fig. 4. The distribution of the compressive forces along the delamination length is plotted for four load levels in Fig. 5.

Geometric Model

Consider a specimen with geometry as depicted in Fig. 1. Furthermore, assume the following features for the specimen configuration: (a) the cantilever beam is considered as a nondelaminated bending beam element prior to application of the critical load, (b) the delaminated part will buckle after the critical load application, (c) the delaminated part can not carry additional axial load but can withstand the shear resultant force and moment after its buckling, and (d) though asymmetry is seen at the two delamination ends, the buckled delamination part is symmetric.

Table 1 Geometry and lay-up configuration of specimens

Specimen # and Lay-Up	Dimensions, L×T×W [mm]	Delamination Length, l [mm]	Delamination depth, h/T	Delamination Position, d [mm]
#1 $[0/90]_{12}$	110×3.7×12.7	50	3/24	55
#2 $[0/90]_{12}$	110×3.7×12.7	50	6/24	55

Table 2 Material properties for Hexcel IM7-8552 graphite/epoxy

Property	Value
Longitudinal Modulus, E_{11}	164.1 GPa (23.8 msi)
Transverse Modulus, E_{22}	11.7 MPa (1.7 ksi)
Shearing Modulus, G_{12}	115.1 MPa (16.7 ksi)
Major Poisson Ratio, ν_{12}	0.3

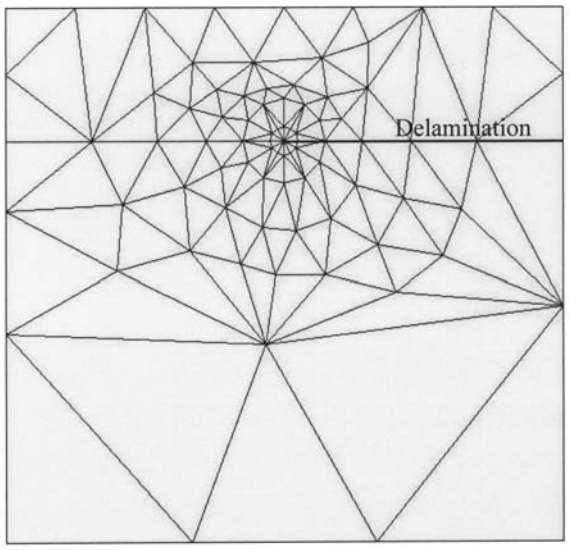

Fig. 2 Singular elements at concentrated point

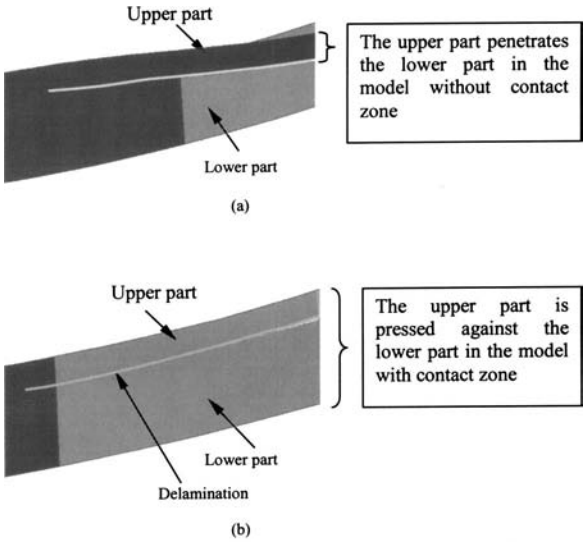

Fig. 3 Situation around the end of delamination: (a) penetration of the delamination flanks without contact analysis; and (b) contact of the delamination flanks with contact analysis.

Based on these features, we can divide the solving procedure into two steps, as shown in Fig. 6. By combining the theories of cantilever bending [19] and stability [20], we obtain the solution for the delaminated cantilever as illustrated in the following paragraphs. Assuming x is the position along the length of the specimen, we identify three distinctive regions as:

1) $0 \leqslant x \leqslant L - l/2$, is the region between the fixed boundary and the delamination, denoted as region I in Fig. 6, in which the out-of-plane deformation, y, and the rotation angle along the normal axis y' are calculated by:

$$y = \frac{1}{6}\frac{P}{WD_b}(L-x)^3 + \frac{1}{2}\frac{P}{WD_b}L^2x - \frac{1}{6}\frac{P}{WD_b}L^3 \qquad (1)$$

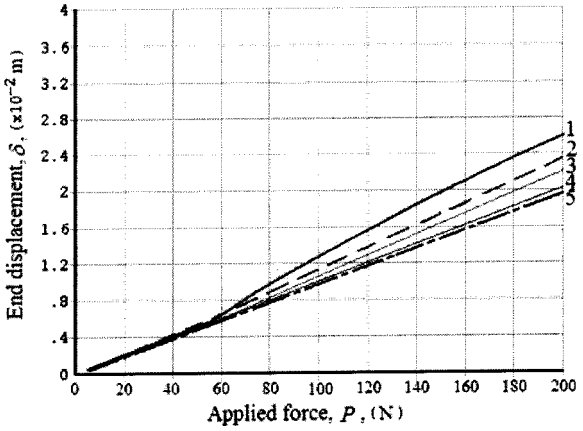

Fig. 4 Relation of load and displacement: Line 1—model for $h/T = 6/24$, without contact zone; Line 2—model for $h/T = 6/24$, with contact zone; Line 3—model for $h/T = 3/24$, without contact zone; Line 4—model for $h/T = 3/24$, with contact zone; and Line 5—model without delamination.

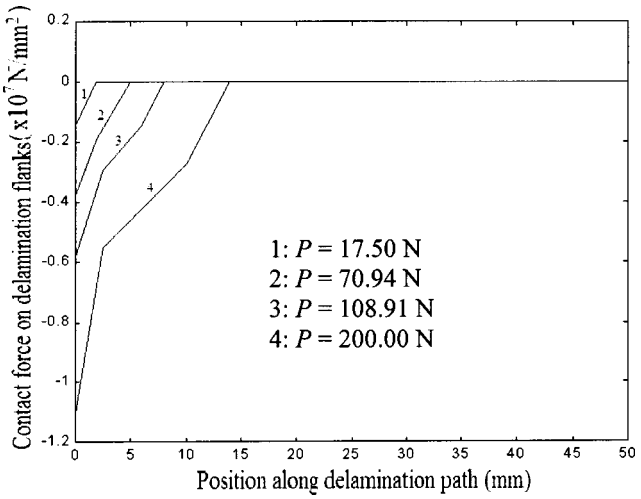

Fig. 5 Distribution of contact force along the delamination: *P*—applied load; Delamination length here is 50 mm.

$$y' = -\frac{1}{2}\frac{P}{WD_b}(L-x)^2 + \frac{1}{2}\frac{P}{WD_b}L^2 x \tag{2}$$

where P is the applied force, W the width of the specimen, L the length of the specimen, and D_b the bending stiffness of the cantilever beam without delamination.

2) $L-l/2 \leqslant x \leqslant L+l/2$, is the region of the delamination, denoted as region *II* in Fig. 6, where the out-of-plane deformation y and the rotation angle along the normal axis y' are:

$$y = \frac{1}{6}\frac{P}{WD_b}(L-x)^3 + \frac{1}{2}\frac{P}{WD_b}L^2 x - \frac{1}{6}\frac{P}{WD_b}L^3 + \frac{\overline{P}}{D_b}\frac{T-h}{4}\left(x-\frac{L-l}{2}\right)^2 \tag{3}$$

$$y' = -\frac{1}{2}\frac{P}{WD_b}(L-x)^2 + \frac{1}{2}\frac{P}{WD_b}L^2 x + \frac{\overline{P}}{D_b}\frac{T-h}{2}\left(x-\frac{L-l}{2}\right) \tag{4}$$

3) $L+l/2 \leqslant x \leqslant L$, is the region following the delamination to the free end of the specimen, denoted as region *III* in Fig. 6, with:

$$y = \frac{1}{6}\frac{P}{WD_b}(L-x)^3 + \frac{1}{2}\frac{P}{WD_b}L^2 x - \frac{1}{6}\frac{P}{WD_b}L^3 + \frac{\overline{P}}{D_b}\frac{T-h}{4}l^2 + \frac{\overline{P}}{D_b}\frac{T-h}{4}\left(x-\frac{L-l}{2}\right)l \tag{5}$$

$$y' = -\frac{1}{2}\frac{P}{WD_b}(L-x)^2 + \frac{1}{2}\frac{P}{WD_b}L^2 x + \frac{\overline{P}}{D_b}\frac{T-h}{2}l \tag{6}$$

where P_0 is the critical load defined as: $P_0 = 4\pi^2 E h^3/12(1-\nu^2)l^2$, and $\overline{P}$ is a combination of geometric quantities, critical and applied loads given by

$$\overline{P} = 6\frac{h}{T}\left(1-\frac{h}{T}\right)\left(\frac{L-l}{T^2}\right)\left(\frac{P}{W}\right) - P_0.$$

Substitute $x=L$ into Eq. (5) in order to obtain the free end displacement, δ:

$$\delta = \frac{1}{3}\frac{P}{WD_b}L^3 + \frac{\overline{P}}{D_b}\frac{T-h}{4}Ll \tag{7}$$

Later, the values of the free end displacement, δ, calculated form Eq. (7) are plotted against the applied load, P. The results are compared with experimental data and with FEM simulations in Fig. 9. As seen, a good agreement exists between all results, i.e., analytical experimental and FEM, up to point B at which crack growth and kinking was developed.

The formulation of the energy release rate, G, of a delaminated cantilever beam as derived by Yin [21], is

$$G = \frac{1-\nu_{13}\nu_{31}}{2ET^3}\left\{\frac{(TP^*)^2}{h(1-h)} + \frac{12(M^*)^2}{\overline{h}^3} + \frac{12(TP^*/2-M^*)}{(1-\overline{h})^3}\right\} \tag{8}$$

where T is the thickness of whole specimen, $\overline{h}$ is the thickness ratio of the delaminated beam to the whole specimen, $\overline{h}=h/T$, and P^* is the equivalent force that produces a singular stress field near the delamination front. Here, we include the effect of the contact zone by introducing the following term for the equivalent force, P^*_{cz}, M^*_{cz} expressed as:

$$P^*_{cz} = 3\frac{h}{T}\frac{1}{W}\left(1-\frac{h}{T}\right)\frac{L}{T}\left(\frac{3}{2}+\frac{\Delta}{L}\right)P - \left(1-\frac{\Delta}{l}\right)P_0 \tag{9}$$

M^* is the equivalent moment in the delaminated part that also produces the singular stress field near the delamination front, and is a function of the moment in the delaminated part, M_3, and the moment in the whole specimen, M_1. M^* is then expressed as follows:

$$M^* = M_3 - M_1\overline{h}^3 \tag{10}$$

The bending moments in the delaminated part and base parts are defined as $M_3 = D_d\theta$, and $M_1 = D_b\theta$, respectively, with D being the corresponding bending-stiffness and θ the change of rotation angle at the delamination front. For an infinitesimal element in front of the delamination tip, assuming the contact zone model, the moment ratio will be

$$\frac{M_3}{M_1} = \frac{D_d}{D_b} = \frac{Eh^3/12(1-\nu^2)}{ET^3/12(1-\nu^2)} = \left(\frac{h}{T}\right)^3 = \overline{h}^3 \Rightarrow M_3 = M_1\overline{h}^3 \tag{11}$$

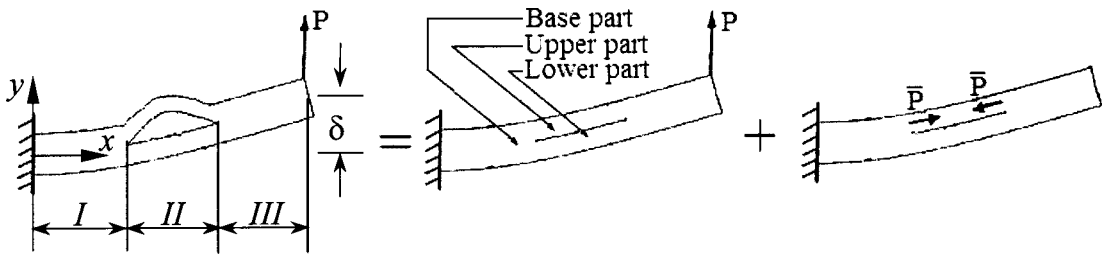

Fig. 6 Procedure of solution to simple geometric model

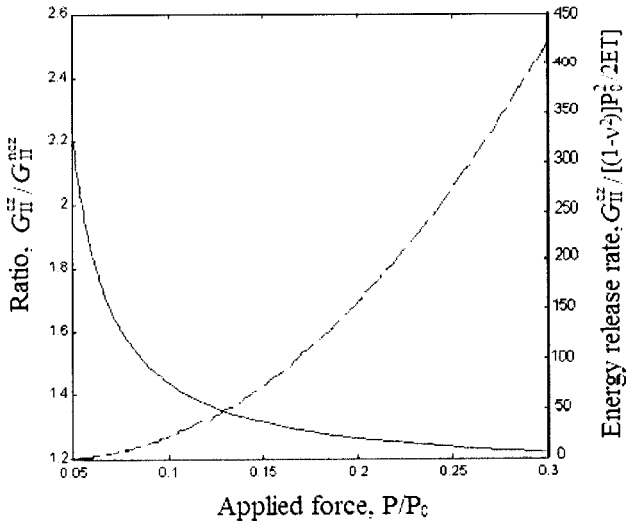

Fig. 7 Variation of energy release rate with applied loading: solid line—ratio of energy release rate with contact zone to that without contact zone; dash line—energy release rate with contact zone.

From the above inference, one can conclude that the equivalent moment, M_{cz}^*, is $M_{cz}^*=0$ at contact zone region. That dictates that any singularity effects in the front of the crack tip may be attributed to the equivalent force, P_{cz}^* only.

The influence of the applied load, P/P_0, in the mode II energy release rate at the presence of contact zone, G_{II}^{cz}, as well as in the case without contact zone, G_{II}^{ncz}, are illustrated in Fig. 7. From the plotted results one can conclude that, the G_{II}^{cz} increases with the applied load, while the combined mode II energy, G_{II}^{cz}/G_{II}^{ncz}, decreases with the applied load. The latter indicates that G_{II}^{ncz} increases faster than G_{II}^{cz}; that is, the specimen is weaker if no contact zone is assumed, since the critical energy release rate value, G_{IIc}, will be achieved sooner.

Experiments

The material used in all specimens was IM7/8552 Hexcel prepreg graphite/epoxy. The material properties are shown in Table 2. Experiments were conducted by using two groups of specimens. All specimens were prepared by hand lay-up and cured according to the manufacturer's curing cycle. Two groups of 24-ply specimens, $[0/90]_{12}$, are fabricated with thickness ratios of $h/T=3/24$ and $h/T=6/24$, i.e., delamination is embedded between the interface of the $3^{rd}/4^{th}$ and the $6^{th}/7^{th}$ plies. The geometric parameters are listed in Table 1. Experiments were performed on an Instron-8852 servo-hydraulic material testing system. Quasi-static loading was applied to the free end of the specimens by a specially modified MMB fixture [22], which guarantees the vertical direction of the transverse loading. The specimen is fixed at the other end. Observation of the specimens and crack recording is performed with a TeLe-Microscopic system (TLM). The experimental setup is shown in Fig. 8.

Results and Discussion

The results of the finite element analysis depicting the effect of quasistatically applied load, P, to the end displacement, δ, at the cantilever beam are illustrated in Fig. 4. Here the following cases are plotted: (1) $h/T=6/24$, without contact zone, (2) $h/T=6/24$, with contact zone, (3) $h/T=3/24$, without contact zone, (4) $h/T=3/24$, with contact zone, and (5) model without delamination. Analysis of the aforementioned results revealed that the structural integrity of the cantilever beams was compromised with increase in the h/T ratio, i.e., compare cases $h/T=3/24$ and $h/T=6/24$. That is the deeper the delamination is located in the beam, the weaker the structure becomes in its resistance to deformation. This result confirms findings from previous studies [3,22] in which the contact zone effect was not considered. For the case with contact zone, we found that the beam with the same geometry is more resistant to the transverse deformation in presence of contact. Similar results were also reported in Ref. [16].

The resultant contact force on the flanks of the delamination versus the position along the delamination path, for a variety of applied loads, P, is plotted in Fig. 5. The calculated contact force had a negative sign at the inner end (the side close to the fixed end of cantilever) of the delamination, which indicates the local compression condition at this end, and zero at the outer end (the side

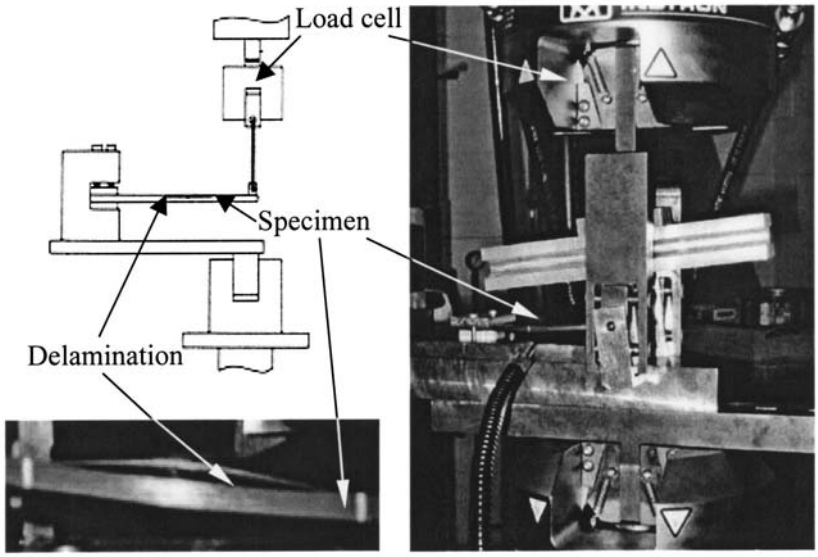

Fig. 8 Experimental setup

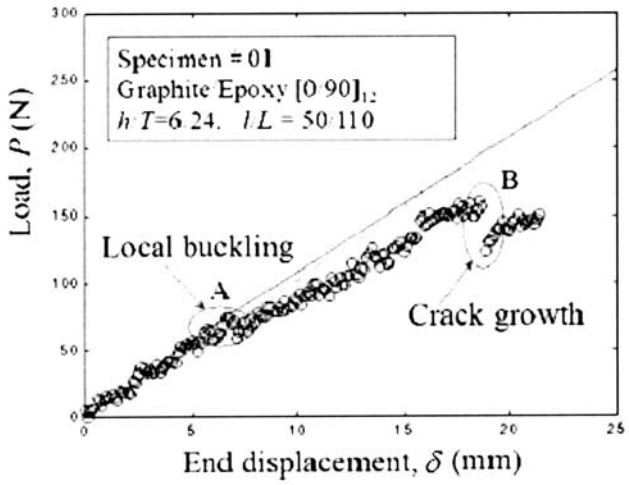

Fig. 9 Applied load, *P*, versus displacement, δ, at the free end of cantilever beam: solid line—geometric model; dashed line—finite element analysis; and circle—experimental data.

close to the free end of cantilever), which indicates the open (mode I) condition. The different local condition will further affect the propagation behavior of cracks that initiate at these points. Figure 5 also illustrates the increase of contact region with applied load increase, e.g., compare plots of $P=17.5$ N versus $P=200$ N.

Figure 9 illustrates the analytical and experimental load-displacement responses of the delaminated cantilever composite beam subjected to transverse loading. As seen here, there are two critical points in the load and end displacement behavior. Point A denotes the occurrence of local buckling, which involves changing the rate of load-displacement response. The analytical and experimental load data of point A are 67.59 N and 69.92 N, respectively, demonstrating a good agreement between analysis and experiment. Point B indicates a sudden decrease of the load due to the initiation and propagation of a crack at one end of delamination.

The contact zone effect on the fracture behavior in terms of the stress intensity factor ratio of mode II over mode I, i.e., K_{II}/K_I, is shown in Fig. 10. The K_{II}/K_I is computed at the delamination ends, namely the left end (see Fig. 5) where the contact zone will be developed, and the right end where there is no significant contact zone. Moreover, K_{II}/K_I calculations are performed for two different lay-up configurations, $h/T=3/24$ (a–d) and $h/T=6/24$ (e–g). Cases (a–b) and (e–f) include the effect of contact zone,

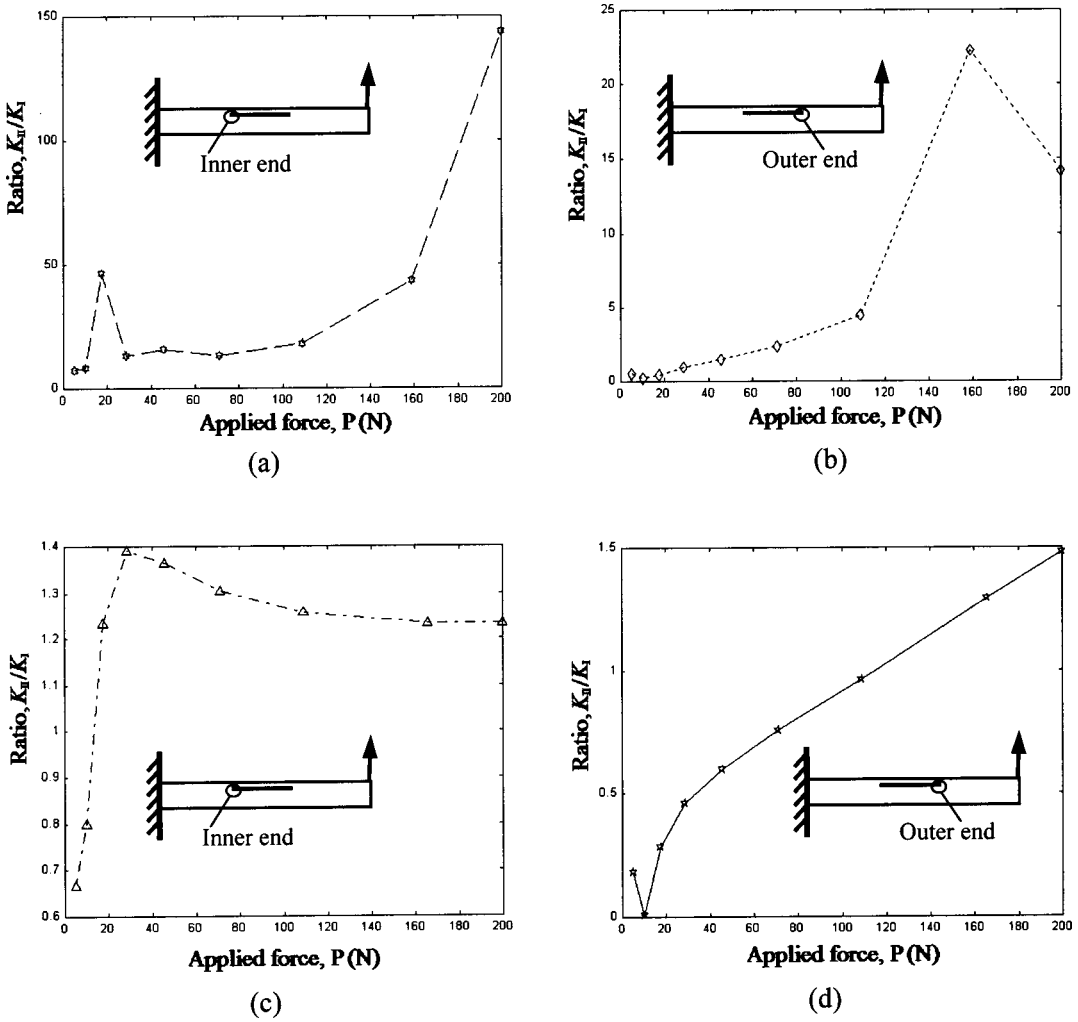

Fig. 10 Ratio of stress intensity factors in mode II to mode I: (*a*) inner end for *h*/T=3/24 with contact zone; (*b*) outer end for *h*/T=3/24 with contact zone; (*c*) inner end for *h*/T=3/24 without contact zone; (*d*) outer end for *h*/T=3/24 without contact zone; (*e*) inner end for *h*/T=6/24 with contact zone; (*f*) outer end for *h*/T=6/24 with contact zone; (*g*) inner end for *h*/T=6/24 without contact zone; and (*h*) outer end for *h*/T=6/24 without contact zone.

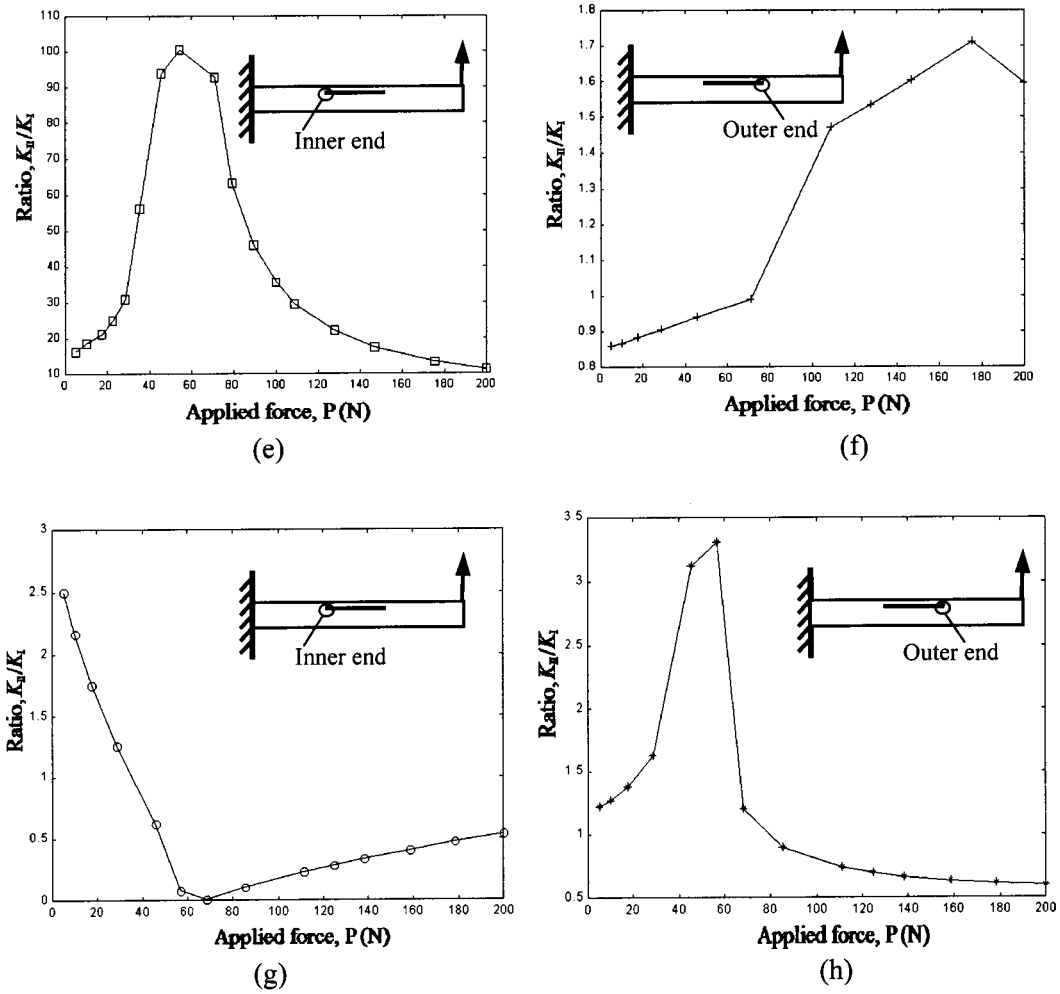

Fig. 10 (***continued***)

while cases (c–d) and (g–h) do not include contact zone. Both lay up configurations while subjected to the effect of contact zone, i.e., Fig. 10 cases (a–b) and (e–f), their fracture behavior at the inner end is dominated by mode II, as the local compressive condition around the inner end (as seen in Fig. 5) causes an apparent contact zone and loses the singularity of mode I at this point, while the singularity due to mode II is present. The large values of K_{II}/K_I in Figs. 10(a) and (e) illustrate the dominance of mode II and the effect of contact zone. The outer delamination ends on Figs. 10(b) and (f), are still in mixed mode condition because of no apparent contact zone. Therefore, modes I and II change in a comparable way with load increase, although the K_{II}/K_I values for the thinner delamination, $h/T=3/24$, are higher. In the model without contact zone, the fracture at both delamination ends operates in mixed mode conditions with comparable effect of mode I and mode II, as seen in Figs. 10 (c–d) for $h/T=3/24$ and (g–h) for $h/T=6/24$.

Furthermore, by comparing Fig. 9 and Figs. 10 (e–h), a change in the K_{II}/K_I ratio is illustrated around the local buckling load, i.e., 69.92 N, denoted as point A in Fig. 9. This change in the K_{II}/K_I behavior signifies two physical phenomena; namely, contact zone and onset of local buckling. Prior to this critical load, only the effect of contact zone was present.

The normalized stress intensity factors in mode I and II, K_I and K_{II}, for $h/T=6/24$ and at the inner end with contact are illustrated in Fig. 11. K_I initially increases followed by a reduction in its values with increasing loading. K_{II} increases monotonically as the load increases. Similar behaviors are also found in Whitcomb [14].

Figure 12 is the image of the delamination crack end for $h/T=6/24$. The delamination is between the 6th (90 deg) and 7th (0 deg) layers. After initiation, the crack kinks into the 6th layer at a large angle until meets the interface between the 5th (0 deg) and the 6th (90 deg) layers. With further load increase, the delamination propagates at the 5th/6th interface. The single steep kinking during propagation suggests the local dominance of mode II again, as mode I dominant fracture is characterized by multiple kinking at an about 45 deg angle, see schematic in Fig. 13. The case of $h/T=3/24$, in which the delamination is located between the 3rd (0 deg) and 4th (90 deg) layers, i.e., $h/T=3/24$, is simple since the crack remains on the same interface during propagation. The above results illustrate the dependence of the crack propagation trajectory on the architectural configuration of specimens.

Conclusions

A nonlinear finite element analysis that accounts for the contact zone effect is presented. The model provides sound results for calculating the mechanical and fracture parameters for a composite cantilever beam with delamination. The solution of geometric model is also derived here for the aforementioned structure.

The finite element analysis for the delaminated composite cantilever beam without contact zone indicated an apparent penetra-

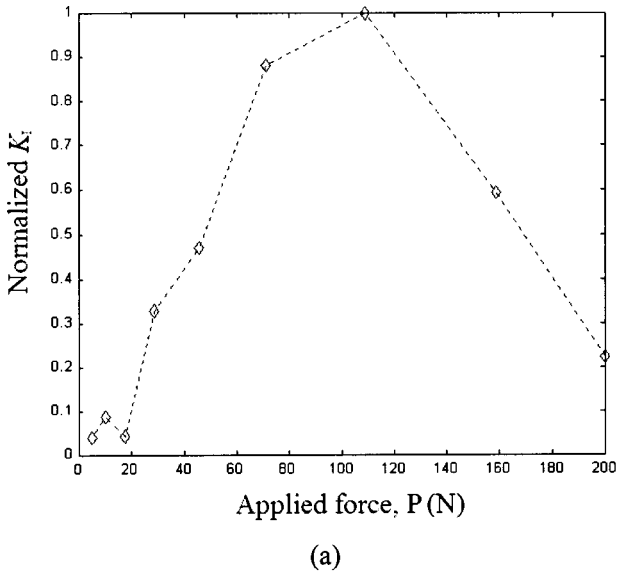

Fig. 11 The variation of stress intensity factor in mode I with loading: (a) mode I, K_I; and (b) mode II, K_{II}.

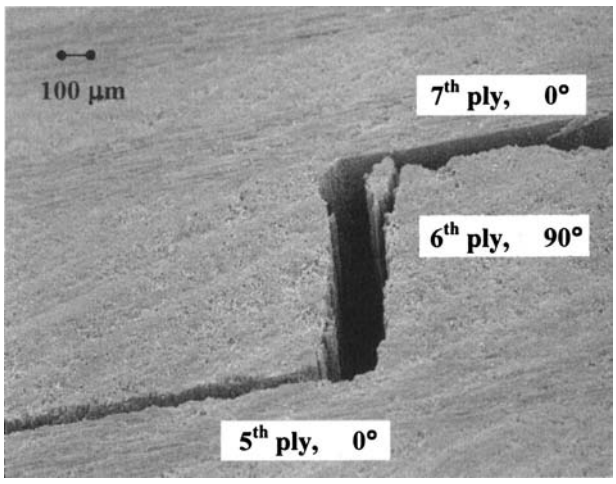

Fig. 12 Trajectory of crack propagation in IM7/8552 graphite/epoxy. Kinking from the 6th/7th to the 5th/6th interface is observed.

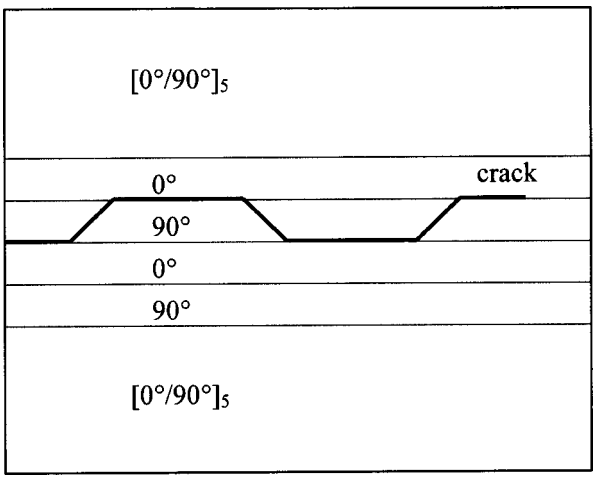

Fig. 13 Trajectory of crack propagation in mode I

tion between the two flanks of the delamination at its inner end, which verified the necessity of considering the effect of contact zone in similar cases. The K_{II}/K_I ratio was utilized to illustrate the effect of contact zone on the fracture behavior.

In the model for a delaminated cantilever beam without contact zone, the fracture at the delamination ends operates in comparable (between the two ends) mixed mode condition. To this extent, performed calculations of K_{II}/K_I illustrated the comparability. In the model with contact zone, there is no significant change for the fracture behavior except at the inner delamination locale, where it is characterized with large contact zone. The significant change is demonstrated by the large value of K_{II}/K_I and its variation with increasing load.

In terms of the facture behavior of the studied structure the existence of contact zone subjects the inner delamination end in an increased mode II (dominant mode), while the noncontact end lies in the comparable K_{II} to K_I mixed mode condition. Dependent on the lay-up architecture of specimens, the crack may undergo multiple kinking, and further propagate on an interface in presence of contact zone.

In terms of the structural integrity, the existence of contact zone on a delamination makes the structure stronger in resistance to deformation, although the effects of the delamination should not be neglected. The future work will focus on the fatigue behavior of delaminated structures under the effect of contact zone.

Acknowledgments

This work was sponsored by the National Science Foundation, Career Award CMS-9982023. The authors gratefully acknowledge this financial support and are thankful to the Program Manager, Dr. Jorn Larsen-Basse for his genuine interest and encouragement.

Nomenclature

D_b = bending stiffness of base part of cantilever
D_d = bending stiffness of the delaminated (upper) part
E = Young's modulus
ν = Poisson's ratio
L = length of whole specimen
T = thickness of whole specimen
W = width of whole specimen
l = delamination length
h = thickness of the delaminated part
P = applied force
δ = transverse displacement
Δ = length of contact zone
P_0 = critical buckling load per unit width of delaminated part

K_I = stress intensity factor in mode I
K_{II} = stress intensity factor in mode I
$\underline{G}$ = energy release rate
P = axial compressive force per unit width of delaminated part

References

[1] Sanford, R. J., 1997, *Foundations of Linear Elastic Fracture Mechanics*, SPIE Optical Engineering Press, Bellingham, Washington, pp. 161–363.
[2] Sanford, R. J., 1997, *Crack Tip Stress Fields*, SPIE Optical Engineering Press, Bellingham, Washington, pp. 3–215.
[3] Sheinman, I., Kardomateas, G. A., and Pelegri, A. A., 1998, ''Delamination Growth During Pre- and Post-Buckling Phases of Delaminated Composite Laminates,'' Int. J. Solids Struct., **35**(1–2), pp. 19–31.
[4] Sheinman, I., and Soffer, M., 1991, ''Post-Buckling Analysis of Composite Delaminated Beams,'' Int. J. Solids Struct., **27**(5), pp. 639–646.
[5] Simitses, G. J., Sallam, S., and Yin, W. L., 1985, ''Effect of Delamination of Axially Loaded Homogeneneous Laminated Plates,'' AIAA J., **23**(4), pp. 1437–1444.
[6] Yin, W. L., Sallam, S. N., and Simitses, G. J., 1986, ''Ultimate Axial Load Capacity of a Delaminated Beam-Plate,'' AIAA J., **24**(1), pp. 123–128.
[7] Kardomateas, G. A., 1989, ''Large Deformation Effect in the Postbuckling Behavior of Composite With Thin Delaminations,'' AIAA J., **27**(5), pp. 624–631.
[8] Suemasu, H., 1993, ''Effect of Multiple Delaminations on Compressive Buckling Behaviors of Composite Panels,'' J. Compos. Mater., **27**, pp. 1172–1192.
[9] Suemasu, T., Kumagai, T., and Gozu, K., 1998, ''Compressive Behavior of Rectangular Composite Laminates With Multiple Circular Delaminations,'' AIAA J., **36**, pp. 1279–1285.
[10] Comninou, M., and Dundurs, J., 1979, ''On the Frictional Contact in Crack Analysis,'' Eng. Fract. Mech., **12**, pp. 117–123.
[11] Comninou, M., and Dundurs, J., 1979, ''An Example for Frictional Slip Progressing Into a Contact Zone of a Crack,'' Eng. Fract. Mech., **12**, pp. 191–197.
[12] Antipov, Y. A., 1995, ''An Interface Crack Between Elastic Materials When There is Dry Friction,'' J. Appl. Math. Mech., **59**(2), pp. 273–287.
[13] Audoly, B., 2000, ''Asymptotic Study of the Interfacial Crack With Friction,'' J. Mech. Phys. Solids, **48**(9), pp. 1851–1864.
[14] Whitcomb, J. D., 1981, ''Finite Element Analysis of Instability Related Delamination Growth,'' J. Compos. Mater., **15**, pp. 403–426.
[15] Moradi, S., and Taheri, F., 1999, ''Postbuckling Analysis of Delaminated Composite Beams by Differential Quadrature Method,'' Compos. Struct., **46**, pp. 33–39.
[16] Yeh, M. K., and Fang, L. B., 1999, ''Contact Analysis and Experiments of Delaminated Cantilever Composite Beam,'' Composites, Part B, **30**(4), pp. 407–414.
[17] Yeh, M. K., Fang, L. B., and Kao, M. H., 1997, ''Bending Behavior of Delaminated Composite Plates With Contact Effects,'' Compos. Struct., **39**(3–4), pp. 347–356.
[18] ANSY Smanual, at http://www.cesup.ufrgs.br/ansys/elem_55/chapter4/ES4-2.htm
[19] Timoshenko, S., 1934, *Theory of Elasticity*, McGraw-Hill, New York, New York, pp. 33–38.
[20] Brush, D. O., and Almroth, B. O., 1975, *Buckling of Bars, Plates, and Shells*, McGraw-Hill, New York, New York, p. 22.
[21] Yin, W. L., and Wang, T. S., 1984, ''The Energy-Release Rate in the Growth of a One-Dimensional Delamination,'' ASME J. Appl. Mech., **51**, pp. 939–941.
[22] Pelegri, A. A., and Chen, I., 2000, ''Mixed Mode Fatigue of Fiber Reinforced Composites Using a Modified MMB Fixture,'' 41st AIAA/ASME/ASCE/AHS/ASC SDM (Structures) Atlanta, AIAA-2000-1404.